RESEARCH ARTICLE
DOI: https://doi.org/10.4038/ouslj.v21i1.7741

OUSL Journal, 2026
Vol. 21, No. 1, (pp. 7-36)

Computational Investigation of HDLP Inhibitors toward Anticancer Drug Design: Molecular Dynamics-Based Binding Energy Evaluation and Binding Pocket Characterization

G. Parthiban[1], R. Dushanan[2], D. P. Dissanayake[3] and R. Senthilnithy[2*]

[1]Department of Chemistry, Eastern University, Sri Lanka
[2]Department of Chemistry, The Open University of Sri Lanka, Sri Lanka
[3]Department of Chemistry, Faculty of Science, University of Colombo, Sri Lanka

Abstract

Histone deacetylases (HDACs) are well-established therapeutic targets in cancer due to their critical roles in regulating histone acetylation, chromatin structure, and gene expression, which are associated with cell growth, differentiation, and apoptosis. This study aims to investigate the binding interactions of hydroxamic acid–based inhibitors against histone deacetylase-like protein (HDLP) using the MM-PBSA method, assess their structural stability, and evaluate their inhibitory potential, employing integrated computational approaches. In this study, SAHA and newly designed derivatives CHR3996, ACY1215, HAD1, and HAD5 were systematically evaluated using

Correspondence should be addressed to **Prof. R. Senthilnithy, Department of Chemistry, The Open University of Sri Lanka, Sri Lanka.*

Email: *rsent@ou.ac.lk*

https://orcid.org/ 0000-0001-9557-8750

(Received 09th February 2026, Revised 20th May 2026, Accepted 30th May 2026, © OUSL)

integrated in-silico drug discovery approaches. Molecular docking was performed to predict binding orientations, key intermolecular interactions, and relative binding affinities toward the HDLP enzyme. To further validate docking results, molecular dynamics simulations were performed to assess the structural stability, compactness, and conformational flexibility of the HDLP–inhibitor complexes under dynamic conditions. Trajectory analyses, including RMSD, radius of gyration, RMSF, solvent-accessible surface area, and Ramachandran plots, indicated improved stability and favourable conformational behaviour for complexes involving SAHA, CHR3996, ACY1215, HAD5, and HAD3. In addition, MM-PBSA binding free energy calculations confirmed that CHR3996, ACY1215, HAD5, and HAD3 exhibit stronger binding affinities compared to the remaining inhibitors. The inhibitory potential of the selected compounds was further assessed by theoretically estimating IC_{50} values from docking-derived binding energies. ACY1215, CHR3996, and SAHA demonstrated the most potent inhibition with predicted nanomolar IC_{50} values, whereas HAD2–HAD4 showed moderate to weak activity. Overall, these findings identify CHR3996, ACY1215, HAD5, and HAD3 as promising HDAC inhibitor candidates for further lead optimization, experimental validation, and preclinical anticancer drug development.

Keywords: *HDAC inhibitors, molecular docking, MD simulation, hydroxamic acid derivatives, epigenetic drug discovery*

Introduction

Epigenetics involves heritable changes in gene expression without altering the DNA sequence, regulated by reversible modifications such as DNA methylation and histone post-translational modifications (acetylation, ubiquitination, phosphorylation) that control chromatin structure and cellular function (Chuang & Jones, 2007). Dysregulation of these mechanisms is strongly linked to cancer, making epigenetic regulators attractive therapeutic targets (Nakao, 2001). Histones, which form nucleosomes by wrapping DNA around octamers, govern DNA accessibility and transcription (Razzak, 2013). Among epigenetic regulators, histone deacetylases (HDACs) remove acetyl groups from lysine residues, promoting chromatin condensation and transcriptional repression of tumor suppressor genes. In contrast, histone acetyltransferases (HATs) acetylate

histones, leading to chromatin relaxation and gene activation (Arkin & Doyle, 2004).

HDAC inhibitors have emerged as promising anticancer agents by restoring acetylation and reactivating silenced genes involved in cell cycle arrest, differentiation, and apoptosis. However, many inhibitors lack isoform selectivity and exhibit dose-limiting toxicities, necessitating the rational design of more effective compounds (Sadri-Vakili & Cha, 2006). Hydroxamic acid–based inhibitors, such as SAHA, represent a potent structural class in HDAC-targeted drug discovery. Structural studies of histone deacetylase-like protein (HDLP), which shares high homology with human HDACs, have provided insights into inhibitor binding, particularly at the catalytic zinc-binding domain (Drazic et al., 2016; Sawatzky et al., 2016).

Despite significant progress in HDLP inhibitor development, a detailed molecular-level understanding of hydroxamic acid interactions with HDLP, including their binding affinity, dynamic stability, and inhibitory potential, remains incomplete. Therefore, the objective of this study is to systematically investigate the binding interactions, structural stability, and energetics of HDLP–hydroxamic acid inhibitor complexes using an integrated computational approach. Molecular docking, molecular dynamics simulations, and MM-PBSA free energy calculations were employed to evaluate the binding behaviour of selected inhibitors.

In addition, theoretical IC_{50} values were estimated to assess their inhibitory potency. This study aims to provide mechanistic insights and a computational framework to support the rational design and optimization of HDLP inhibitors for anticancer drug development.

Methodology

The three-dimensional crystal structure of the histone deacetylase-like protein (HDLP; PDB ID: 1ZZ1 - Figure 1) was obtained from the Protein Data Bank and processed using UCSF Chimera (Nielsen et al., 2005). All water molecules, ligands, and ions were deleted, except for the essential zinc and potassium ions, to prepare the enzyme for subsequent computational analyses.

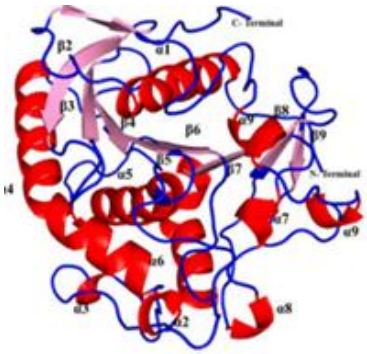

Figure 1. The 3D crystal structure of HDLP shows α-helices in red, β-sheets in violet, and loops in blue

HDLP inhibitors were visualized using Avogadro and optimized with the CBS-QB3 method in Gaussian 09 to calculate accurate molecular energies (Frisch et al., 2009). Optimized structures were converted to .pdb format for docking and further simulations. The inhibitors studied include SAHA, HAD1–HAD5, ACY1215, and CHR3996 (Table 1, Figure 2).

Table 1. *IUPAC nomenclature of the selected HDAC inhibitors*

IUPAC name	Compound Code
Suberoylanilide hydroxamic acid	SAHA
N-hydroxy-3-phenylprop-N-hydroxybenzamide	HAD1
N-hydroxy-3-phenylprop-2-enamide	HAD2
N-hydroxy-3-(pyridin-2-yl)prop-2-enamide	HAD3
N-hydroxy-3-(pyridin-3-yl)prop-2-enamide	HAD4
4-(diphenylamino)-N-(5-(hydroxyamino)-5-oxopentyl)benzamide	ACY1215
2-(6-(((6-fluoronaphthalen-2-yl)methyl)amino)-3-azabicyclo[3.1.0]hex-3-yl)-N-hydroxypyrimidine-5-carboxamide	CHR3996
N-(3-aminopropyl)-N-hydroxy-2-((naphthalen-1-yloxy)methyl)oct-2-enediamide	HAD5

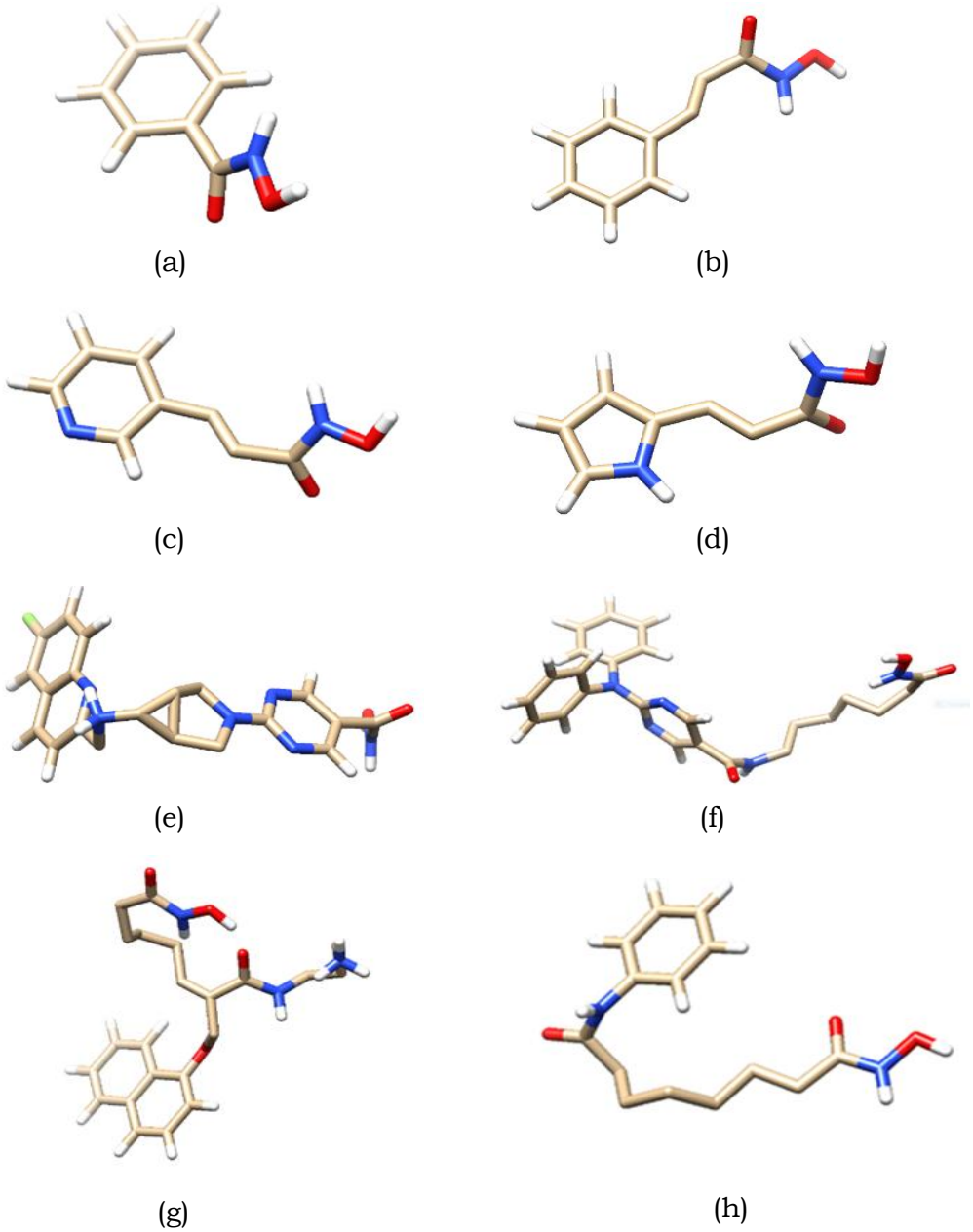

Figure 2. Optimized molecular structures of the HDAC inhibitors studied: (a) HAD1, (b) HAD2, (c) HAD3, (d) HAD4, (e) CHR3996, (f) ACY125, (g) HAD5, and (h) SAHA

Molecular docking studies were carried out using AutoDock Tools 1.5.6, with rotatable bonds adjusted to enhance ligand flexibility, and complexes were visualized in PyMOL (Therrien et al., 2014). The

highest-ranking complexes were selected as initial structures for molecular dynamics simulations.

MD simulations were performed using GROMACS 4.5.6 (Van Der Spoel et al., 2005) with the GROMOS53a6 force field and PRODRG-generated parameters (Oostenbrink et al., 2005). Systems were solvated in cubic boxes with ~20,000 SPC/E water molecules, neutralised with Na^+ ions, and energy-minimised for 500 steps. Equilibration was performed for 100 ps at 300 K and 1 bar using the Leap-frog and Berendsen algorithms (Schüttelkopf & Van Aalten, 2004). Production MD runs lasted 100 ns with a 0.002 ps time step, saving trajectories every 1 ps (Anbarasu & Jayanthi, 2018; Priyani et al., 2021). The trajectories were analysed using RMSD, RMSF, radius of gyration, solvent-accessible surface area, hydrogen-bond analysis, Ramachandran plots, dihedral-angle monitoring, and total-energy calculations (Dushanan et al., 2022a; Parthiban et al., 2022). Quantum chemical structures were visualised using RasMol, PyMOL, and Chimera (Dushanan et al., 2022c).

Interaction and binding energies were computed using GROMACS and MM-PBSA methods:

$$I = 4\varepsilon[(\sigma/r)^{12} - (\sigma/r)^{6}] + \frac{e^2}{4\pi\varepsilon_0 r}$$

$$\Delta G_{binding} = \Delta G_{elec} + \Delta G_{vdW} + \Delta G_{PB} + \Delta G_{SA}$$

Protein structure validation was performed using ProteinsPlus to assess structural integrity and active-site properties (Agnihotry et al., 2022). Hydroxamic acid derivatives were further screened using the Glide module in Schrödinger Maestro, and ADMET properties were analysed using QikProp (Friesner et al., 2004).

The theoretical IC_{50} values of the selected HDLP inhibitors were estimated using their computed binding free energies obtained from molecular docking simulations. The binding free energy (ΔG_{bind}) was converted into an inhibition constant (K_i) using the thermodynamic relation:

$$\Delta G_{bind} = RT\ln K_i$$

where R is the universal gas constant and T is the temperature (298 K). The obtained K_i values were then converted into approximate IC_{50} values using the Cheng–Prusoff relation (Wu et al., 2025):

$$IC_{50} = K_i \left[1 + \frac{[S]}{K_m}\right]$$

For competitive inhibition conditions, where the substrate concentration $[S]$ is significantly lower than K_m, the equation reduces to:

$$IC_{50} \approx K_i = e^{\frac{\Delta G_{bind}}{RT}}$$

Thus, the theoretically obtained ΔG_{bind} values were used to estimate IC_{50} values approximately, enabling potency comparisons among inhibitors prior to experimental validation.

Results and Discussion

Molecular dynamics (MD) simulations were performed to assess the stability, conformational flexibility, and binding interactions of hydroxamic acid derivatives with the HDLP enzyme in aqueous solution. Comparative studies included the HDLP-inhibitor complexes, the HDLP bound to SAHA (Suberoylanilide hydroxamic acid, a reference inhibitor), and the unbound HDLP enzyme.

Screening of hydroxamic acid derivatives

All hydroxamic acid derivatives were screened using the QikProp module in Maestro to evaluate their ADMET profiles. Descriptors based on Lipinski's rule of five and rule of three were applied to identify compounds with drug-like properties. Compounds meeting the criteria outlined in Table 2 were selected for further analysis.

Table 2. *Predicted ADMET characteristics and their reference values*

Descriptor	Description	Recommended range
mol_MW	The molecular weight of the molecule	< 500
QPlogPo/w	Predicted octanol/water partition coefficient	< 5
DonorHB	The estimated number of hydrogen bonds that the solute would donate to water molecules in an aqueous solution.	≤ 5

AcceptHB	The solute would accept an estimated number of hydrogen bonds from water molecules in an aqueous solution.	≤ 10
Sum of O and N	The number of nitrogen and oxygen atoms.	< 10

Ligands satisfying Lipinski's rules are typically considered drug-like, as they conform to essential pharmacokinetic and physicochemical criteria. Accordingly, in the present study, these ligands were identified as potential HDLP inhibitors based on their druggable properties.

Table 3. *Overview of the results obtained from the QikProp analysis*

Title	mol_MW	QPlog Po/w	Donor HB	Accept HB	N+O	QPlogS	QPPCaco
SAHA	264.324	0.743	3	6.7	5	-2.111	109.106
HAD1	137.138	0.568	2	4.7	3	-1.52	356.419
HAD2	165.191	0.678	2	6.7	5	-1.399	133.267
HAD3	166.179	0.725	2	5.7	4	-1.091	265.739
HAD4	156.184	0.624	3	6.2	5	-1.00	140.88
CHR3996	435.525	0.654	3	7.6	8	-4.616	101.695
ACY1215	396.423	0.789	3	7.7	8	-5.206	106.478
HAD5	389.456	0.743	3	6.7	5	-2.111	109.106

Table 3 summarizes QikProp results for all hydroxamic acid derivatives, including molecular weight, lipophilicity (QPlogPo/w), hydrogen-bond donors/acceptors, heteroatom count (N + O), solubility (QPlogS), and predicted permeability (QPPCaco). Most compounds comply with Lipinski's rules, indicating drug-like properties. SAHA and all derivatives meet basic oral drug-likeness criteria. CHR3996 and ACY1215 stand out for their higher heteroatom counts and acceptable permeability, highlighting their potential as promising HDLP inhibitors. Compared to SAHA, CHR3996 shows

particularly favourable heteroatom content and permeability, supporting its selection for further MD-based evaluation.

Docking analysis of selected inhibitors

The energy-minimized inhibitors were docked into the HDLP enzyme using the Schrödinger XP docking protocol in Maestro. The resulting docked poses and key interactions within the active site are illustrated in Figure 3. The key docking scores and energetic parameters obtained from XP docking are summarized in Table 4. These values

provide a quantitative comparison of binding affinity and predicted interaction strength of each inhibitor toward the HDLP enzyme.

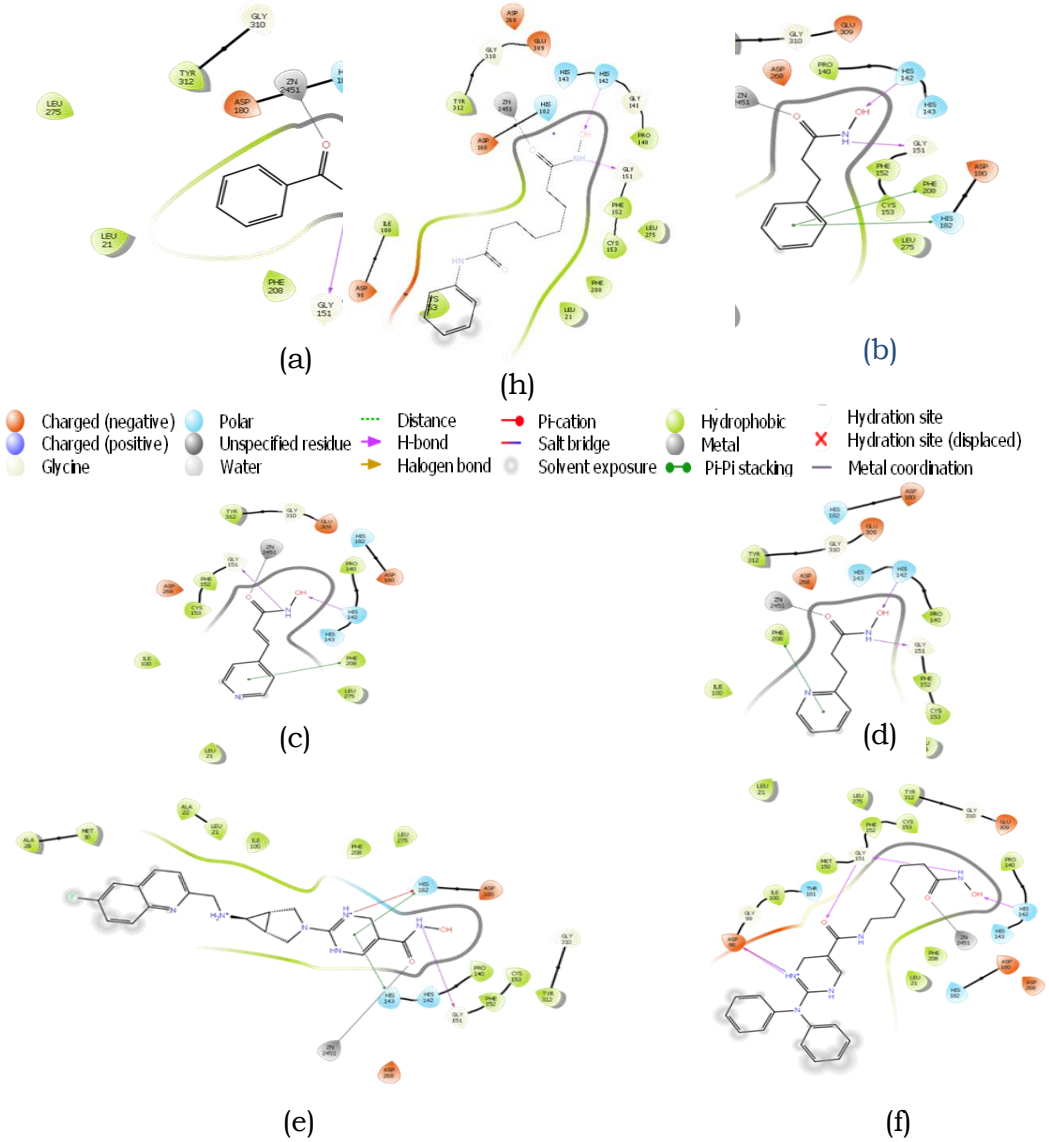

Figure 3. Docking poses and interaction diagrams of the HDLP complexes with (a) HAD1, (b) HAD2, (c) HAD3, (d) HAD4, (e) CHR3996, (f) ACY1215, and (g) SAHA

Docking results showed that hydrogen bonding was the dominant interaction stabilising the HDLP–inhibitor complexes. Among the compounds studied, CHR3996, ACY1215, HAD2, and HAD3 showed comparatively stronger hydrogen-bond interactions within the HDLP active site. This indicates stronger and more favourable binding orientations for these inhibitors. The increased hydrogen-bond contacts may therefore contribute to their improved predicted affinity compared to the remaining hydroxamic acid derivatives. These results highlight the potential of these four compounds as promising HDLP inhibitors, warranting further investigation through molecular dynamics simulations and binding free-energy analysis.

Table 4. *XP docking study parameters and the corresponding binding energy values*

Inhibitor	**DS[a]**	**GS[b]**	**Evdw[c]**	**Ecoul[d]**	**Emodel[e]**	**Energy[f]**
SAHA	-5.134	-5.134	-34.171	-13.452	-61.689	-47.623
HAD1	-6.296	-6.296	-18.351	-12.071	-56.556	-22.423
HAD2	-8.705	-8.705	-25.181	-12.884	-63.053	-32.065
HAD3	-8.584	-8.584	-25.758	-13.052	-63.992	-36.81
HAD4	-7.067	-7.067	-19.298	-12.153	-45.257	-21.851
CHR3996	-8.689	-8.689	-33.897	-13.237	-67.022	-42.261
ACY1215	-8.868	-8.868	-36.025	-13.918	-69.216	-52.235

[a] docking score; [b] glide score; [c] glide van der Waals energy; [d] glide coulombic energy; [e] glide model energy; [f] glide energy.

Table 4 presents the XP docking energies of hydroxamic acid derivatives with HDLP. Lower scores indicate stronger binding. Several derivatives, including HAD2 (-8.70), HAD3 (-8.58), CHR3996 (-8.69), and ACY1215 (-8.86), showed higher predicted affinity than SAHA (-5.13 kcal/mol). These compounds also had lower van der Waals energies, reflecting stable non-covalent interactions. ACY1215 exhibited the strongest binding (-52.23 kcal/mol), followed by CHR3996 (-42.26 kcal/mol). Enhanced hydrophobic packing and hydrogen-bonding interactions explain their superior affinity, and CHR3996, ACY1215, HAD2, and HAD3 are identified as the top HDLP binders for subsequent MD simulations and free-energy analyses.

Table 5. *Binding Gibbs free energies (kJ·mol⁻¹) of the selected potent HDLP inhibitors with the HDLP enzyme*

Inhibitor	ECoul[a]	ECov[b]	EHbond[c]	ELipo[d]	ESolv[e]	Evdw[f]	$\Delta G_{bind}^{[g]}$
SAHA	-11547.55	1695.39	-1999.97	-152.2	-2209.53	-1278.39	-41.53
HAD1	-11531.89	1692.62	-2001.36	-142.6	-2208.29	-1273.99	-16.78
HADd2	-11543.3	1689.62	-2001.94	-146.2	-2208.91	-1274	-28.05
HAD3	-11603.02	1695.1	-2000.15	-146.9	-2208.93	-1269.32	-30.78
HAD4	-11564.99	1685.25	-2002.11	-141.5	-2209.36	-1306.43	-21.27
CHR3996	-11514.68	1696.47	-1991.61	-149.3	-2215.3	-1308.98	-42.45
ACY1215	-11550.85	1772.1	-1992.16	-152.7	-2213.65	-1326.62	-46.41

[a] coulombic energy; [b] covalent energy; [c] hydrogen bond energy; [d] lipophilic energy; [e] generalized Born electrostatic solvation energy; [f] van der Waals energy; [g] binding free energy.

Table 5 shows the binding free energies (ΔG_bind) of HDLP–inhibitor complexes. Lower ΔG_bind indicates stronger stability. SAHA recorded –41.53 kJ/mol, while ACY1215 (–46.41 kJ/mol) and CHR3996 (–42.45 kJ/mol) exhibited the most favourable binding, surpassing SAHA. HAD2 (–28.05 kJ/mol) and HAD3 (–30.78 kJ/mol) also showed improved binding over HAD1 and HAD4, consistent with docking results. Significant negative contributions from Coulombic, hydrogen bonding, and van der Waals interactions indicate that electrostatic and dispersion forces primarily stabilize the complexes. The correlation between docking scores and ΔG_bind confirms that ACY1215, CHR3996, HAD2, and HAD3 are the most potent HDLP inhibitors among the tested derivatives.

Root mean square deviation (RMSD)

RMSD analysis of the HDLP backbone was performed to assess the structural stability of the enzyme when complexed with the selected inhibitors (Dushanan et al., 2021). Overall, the RMSD profiles remained stable throughout the simulation, indicating no significant structural deviations. Slightly higher RMSD fluctuations are observed in some regions due to weaker interactions with nearby residues and the co-factor surroundings, resulting in localized conformational flexibility. The RMSD patterns shown in Figure 4 and S1 confirm that the HDLP-inhibitor systems remained structurally stable under simulation conditions.

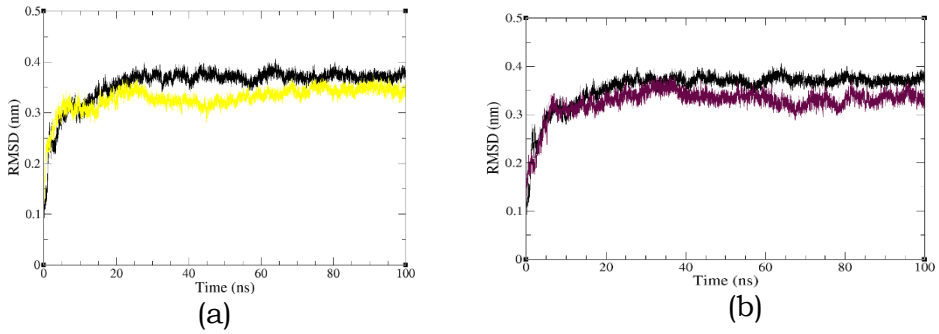

Figure 4. Backbone RMSD profiles of the HDLP enzyme in complex with (a) CHR3996 and (b) HAD5. The black curve in each panel represents the RMSD of the wild-type HDLP.

Figure 4 shows RMSD distributions for all HDLP complexes. Average RMSD values (nm) were: SAHA 0.30, HAD1 0.41, HAD2 0.35, HAD3 0.30, HAD4 0.44, ACY1215 0.30, CHR3996 0.30, HAD5 0.30; wild-type HDLP was 0.36. Lower RMSD indicates greater structural stability. The stability ranking is: HAD3 = ACY1215 = CHR3996 = HAD5 = SAHA > HAD2 > HAD1 > HAD4, indicating that HAD3, ACY1215, CHR3996, HAD5, and SAHA form the most stable HDLP complexes, with minimal backbone fluctuations.

Radius of gyration (Rg)

The radius of gyration (Rg) measures protein compactness and structural stability. Lower, stable Rg values indicate a well-folded structure, while fluctuations suggest unfolding or reduced compactness (Dushanan et al., 2022b). Figure 5 shows Rg trends for the HDLP complexes over the simulation period.

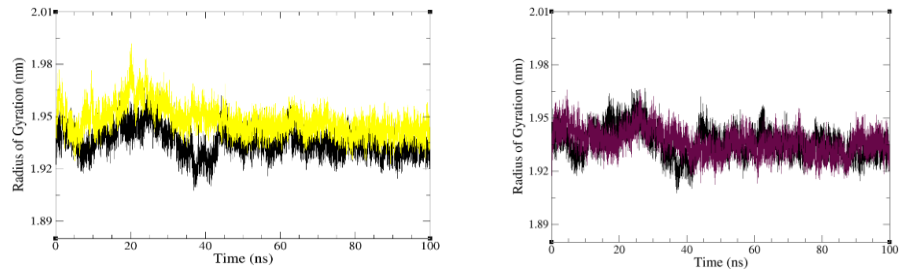

(a) (b)

Figure 5. Radius of gyration profiles of the HDLP enzyme in complex with (a) CHR3996 and (b) HAD5. The black curve in each panel denotes the Rg of the wild-type HDLP.

Figure 5 shows average Rg values (nm) for HDLP complexes: 1.94 (SAHA), 1.96 (HAD1), 1.95 (HAD2), 1.94 (HAD3), 1.96 (HAD4), 1.94 (ACY1215), 1.94 (CHR3996), and 1.94 (HAD5). These results indicate that HDLP maintains a compact structure upon inhibitor binding, with most complexes (SAHA, HAD2, HAD4, ACY1215, CHR3996, HAD5) fluctuating less than 0.1 nm, reflecting stable conformational behavior. The wild-type enzyme also showed a Rg of 1.94 nm, confirming that binding does not alter overall compactness.

Solvent-accessible surface area (SASA)

The solvent-accessible surface area (SASA) reflects protein folding, surface exposure, and structural stability (Dushanan et al., 2025).

Figure 6 shows SASA profiles for HDLP complexes, where variations indicate changes in surface exposure and conformational adjustments upon inhibitor binding.

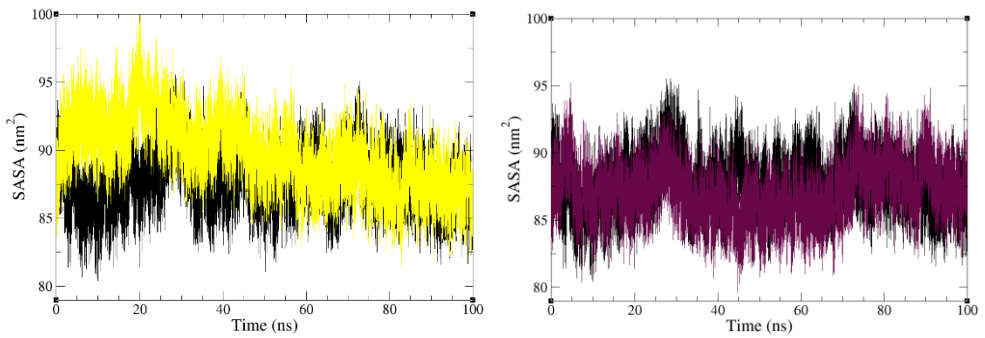

(a) (b)

Figure 6. Solvent-accessible surface area profiles of the HDLP enzyme in complex with CHR3996 and HAD5. The black curve in each panel represents the SASA of the wild-type HDLP

Figure 6 shows that SASA values of all HDLP complexes remained stable during the 100 ns MD simulation. Average SASA values (nm^2) were: SAHA 88.30, HAD1 85.10, HAD2 87.65, HAD3 87.90, HAD4 86.80, CHR3996 90.85, ACY1215 89.68, HAD5 89.38; wild-type HDLP was 87.67. Minimal variations indicate that the complexes retain structural stability and surface exposure, with ACY1215 showing the highest SASA. Overall, inhibitor binding does not significantly affect HDLP's structural integrity.

Root mean square fluctuation (RMSF)

RMSF analysis evaluated residue-level flexibility of wild-type HDLP and HDLP–inhibitor complexes using 100 ns of MD simulation. Figure 7 plots RMSF versus residue number, highlighting residue-specific dynamics and structural mobility upon inhibitor binding.

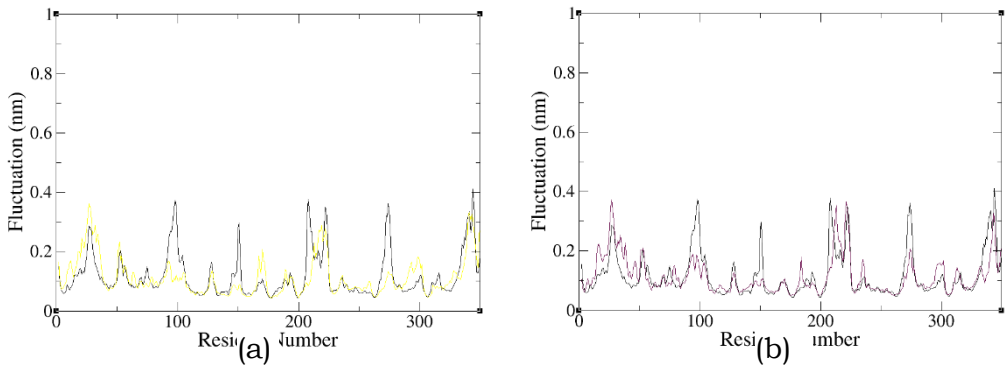

Figure 7. RMSF profiles of amino acid residues in the HDLP enzyme compared with those in the (a) HDLP–CHR3996 and (b) HDLP–HAD5 complexes. The black curve in each panel represents the RMSF of the wild-type HDLP.

RMSF analysis showed that all HDLP complexes have comparable residue-level flexibility. Active site residues (His145, His146, His183, Gly154, Glu103, Gln254, Asp104, Tyr297, Tyr308) exhibited minimal fluctuations, indicating stabilisation upon inhibitor binding. Average RMSF values (nm) were: wild-type 0.120; SAHA 0.116, HAD1 0.151,

HAD2 0.121, HAD3 0.120, HAD4 0.150, ACY1215 0.117, CHR3996 0.119, HAD5 0.122 (Figure 7)**.** ARG29 fluctuated more in HAD1 and HAD4. Overall, lower RMSF at key residues correlates with stronger binding and increased complex stability, showing that inhibitor binding stabilises the HDLP active site.

Interaction energy analysis

Average interaction energies between HDLP and inhibitors were calculated from Lennard-Jones long-range (L-JLR), Lennard-Jones short-range (L-JSR), and Coulombic short-range (CoulSR) contributions, capturing key non-bonded dispersion and electrostatic interactions. The results for each complex are summarised in Table 6**.**

Table 6. *Components of interaction energy and the overall binding energy between HDLP and the inhibitors*

Complex	L-JSR (kJ/mol)	L-JLR (kJ/mol)	CoulSR (kJ/mol)	Interaction energy (kJ/mol)
HDLP-HAD1	-152.06±1.70	-3.92±0.02	116.57±0.59	-39.41±2.20
HDLP-HAD2	-107.38±1.60	17.95±4.20	-3.34±0.02	-92.77±3.30
HDLP-HAD3	-101.96±2.40	-2.74±0.04	-4.65±0.56	-109.36±2.90
HDLP-HAD4	-120.61±1.90	51.32±3.80	-3.04±0.01	-72.32±3.90
HDLP-ACY1215	-125.96±1.40	-98.42±3.00	-4.32±0.05	-228.70±3.80
HDLP-CHR3996	-120.89±1.10	-195.55±1.40	-3.58±0.04	-320.02±7.50
HDLP-HAD5	-149.88±1.30	-70.34±6.50	-4.31±0.04	-224.53±6.50
HDLP-SAHA	-59.33±1.40	-3.25±0.04	-83.78±2.90	-146.36±1.60

Table 6 presents HDLP–inhibitor interaction energies. CHR3996 showed the most negative total energy (−320.02 kJ/mol), followed by ACY1215 (−228.70) and HAD5 (−224.53), indicating stronger non-bonded interactions and stable complex formation. CHR3996's

stability is driven mainly by favourable Lennard-Jones long-range interactions, reflecting deeper engagement of the cavity. HAD1 and HAD4 exhibited weaker interactions, correlating with less stable binding. These results align with docking trends, highlighting CHR3996, ACY1215, and HAD5 as the top HDLP inhibitors.

MM-PBSA free energy analysis

The MM-PBSA method provides a more accurate estimate of binding affinity than average interaction energies. It was used to calculate binding free energies of HDLP–inhibitor complexes with the g_mmpbsa module in GROMACS. The results for all inhibitors are summarised in Table 7**.**

Table 7. *MM-PBSA energy components and the total binding free energies of the inhibitors with the HDLP enzyme*

HDLP Complex	Van der Waals energy (kJ/mol)	Electrostatic energy ΔGelec (kJ/mol)	Polar solvation energy (kJ/mol)	SASA energy (kJ/mol)	Binding free energy (kJ/mol)
HAD1	-0.46±10.09	-156.39±4.68	79.48±6.92	-2.73±0.33	-80.10±7.39
HAD2	125.08±12.46	-152.69±7.72	94.01±11.10	-13.19±0.69	-196.94±12.68
HAD3	65.93±16.25	-699.85±17.40	392.86±9.22	-4.22±0.19	-245.28±8.97
HAD4	114.70±17.08	-71.36±8.20	115.59±15.98	-12.75±0.45	-83.21±5.80
ACY1215	97.75±17.12	-976.70±11.30	492.53±7.90	-4.65±0.46	-391.07±7.70
CHR3996	128.44±13.38	-1058.92±15.89	461.12±11.59	-5.97±0.35	-475.33±14.92
HAD5	101.00±16.08	-944.40±12.68	485.76±6.62	-5.10±0.38	-362.80±10.91
SAHA	75.03±12.10	-826.25±15.37	439.10±5.73	-4.04±0.72	-316.16±7.78

Table 7 summarises MM-PBSA binding energies for HDLP–inhibitor complexes. CHR3996 showed the highest affinity (−475.33 kJ/mol), followed by ACY1215 (−391.07) and HAD5 (−362.80), mainly driven by favourable electrostatic interactions that offset polar solvation penalties. SAHA also bound strongly (−316.16 kJ/mol), while HAD1, HAD2, HAD3, and HAD4 exhibited lower affinities. These results highlight the key role of electrostatics in stabilising HDLP–inhibitor complexes and identify CHR3996 as the strongest binder.

Correlation of MD stability parameters with MM-PBSA binding energies

The relationship between MD stability descriptors and MM-PBSA binding free energies for HDAC–inhibitor complexes is summarised in Table 8.

Table 8. *MD stability parameters with MM-PBSA binding energies*

HDLP Complex	RMSD	Rg	SASA	RMSF	Interaction energy (kJ/mol)	MM-PBSA Binding free energy(kJ/mol)
SAHA	030	1.94	88.30	0.116	-146.36	-316.16
HAD1	0.41	1.96	85.10	0.151	-39.41	-80.10
HAD2	0.35	1.95	87.65	0.121	-92.77	-196.94
HAD3	0.30	1.94	87.90	0.120	-109.36	-245.28
HAD4	0.44	1.96	86.80	0.150	-72.32	-83.21
CHR3996	0.30	1.94	90.85	0.117	-228.70	-391.07
ACY1215	0.30	1.94	89.68	0.119	-320.02	-475.33
HAD5	0.30	1.94	89.38	0.122	-224.53	-362.80

Although RMSD, radius of gyration (Rg), solvent accessible surface area (SASA), and RMSF were discussed individually, their collective trends show a clear correlation with the MM-PBSA binding free energies. Complexes exhibiting lower RMSD and RMSF values, such as ACY1215-HDAC, CHR3996-HDAC, HAD5-HDAC, and HDAC–SAHA, display more negative MM-PBSA binding free energies, indicating enhanced structural stability and stronger binding. The relatively stable Rg values observed across these complexes suggest that protein compactness is maintained upon ligand binding, consistent with favourable binding energetics. In addition, moderate to high SASA values in firmly bound complexes reflect improved ligand burial and a larger protein–ligand contact surface. In contrast, complexes with higher RMSD and RMSF values, such as HAD1-HDAC and HAD4-HDAC, show weaker MM-PBSA binding energies, indicating reduced stability. Overall, these results demonstrate that enhanced conformational stability and reduced flexibility correlate well with stronger binding free energies, validating the quality of the HDLP–inhibitor interactions.

Proteins Plus: A web-based platform for structural analysis of HDLP

The ProteinsPlus web portal was used to analyse HDLP structural features and protein–ligand interactions, including protonation-state analysis, binding-pocket identification, docking, and interpretation of simulation results. Table 9 summarises *the number of elements within the binding pockets*, Table 10 lists functional groups, and Table 11 shows amino acid composition. Together, these results provide detailed insights into HDLP–inhibitor interactions.

Table 9. *Size and shape descriptors of binding pockets of HDLP-inhibitor complexes*

	HAD1	**HAD2**	**HAD3**	**HAD4**	**ACY1215**	**CHR3996**	**HAD5**	**SAHA**
Volume [Å^3]	1378.18	1147.81	989.74	1203.55	720.77	702.64	771.94	742.46
Surface [Å^2]	1224.90	998.80	917.76	1007.97	736.00	768.67	798.63	749.85

Depth [Å]	18.11	23.94	23.75	22.32	30.02	32.46	29.97	24.49
Ellipsoid main axis ratio c/a	0.12	0.13	0.15	0.13	0.14	0.11	0.16	0.11
Ellipsoid main axis ratio b/a	0.26	0.29	0.28	0.25	0.35	0.30	0.31	0.30
Enclosure	0.10	0.11	0.16	0.19	0.17	0.12	0.14	0.12

Table 9 presents HDLP binding pocket descriptors for hydroxamic acid inhibitors. CHR3996 and ACY1215 showed the smallest volume and surface area, with the deepest pockets (32.46 Å and 30.02 Å), indicating tight binding. At the same time, HAD1 had the highest volume and the shallowest depth, indicating weaker complementarity. Enclosure-to-ellipsoid ratios suggest a favourable geometric fit for CHR3996, ACY1215, and HAD5. These trends align with binding free energy and interaction analyses, confirming that compact, deep pockets enhance the stability of complexes.

Table 10. *Number of elements within the binding pockets of the HDLP–inhibitor complexes*

	HAD1	**HAD2**	**HAD3**	**HAD4**	**ACY1215**	**CHR3996**	**HAD5**	**SAHA**
Number of pocket atoms	205	244	251	90	293	285	267	173
Number of carbons (C)	126	139	188	61	188	191	206	115

Number of nitrogen (N)	40	53	37	14	49	42	26	22
Number of oxygens (O)	36	48	22	13	54	48	35	32
Number of sulfurs (S)	2	3	3	1	1	3	0	3
Number of other elements	1	1	1	1	1	1	0	1

Table 10 shows the elemental composition and atom count within the binding pockets of the HDLP–inhibitor complexes. ACY1215, CHR3996, and HAD5 exhibited the largest pocket sizes, with atom counts of 293, 285, and 267, respectively, indicating a more spacious and chemically diverse environment for ligand accommodation. In contrast, HAD4 possessed the smallest pocket (90 atoms), reflecting a more restricted binding region. Carbon was the predominant element across all pockets, followed by nitrogen and oxygen, indicating that non-polar residues predominate, with polar heteroatoms supporting intermolecular recognition. The presence of sulfur in most systems suggests potential for specific thiol or thiolate-associated interactions in certain complexes. Overall, variations in size and heteroatom distribution support differences in structural adaptability and ligand compatibility among the HDLP binding pockets.

Table 11. *Functional group composition of HDLP–inhibitor binding pockets*

	HAD1	**HAD2**	**HAD3**	**HAD4**	**ACY1215**	**CHR3996**	**HAD5**	**SAHA**
Number of hydrogen bond donors	17	21	22	10	32	36	28	16
Number of hydrogen bond acceptors	30	47	52	27	95	91	68	62
Number of metals	1	1	1	1	1	1	1	1
Number of hydrophobic interactions	54	88	43	31	54	40	14	46
hydrophobicity ratio	0.36	0.42	0.42	0.45	0.30	0.27	0.17	0.37

Table 11 shows notable variation in the distribution of functional groups among the HDLP–inhibitor complexes. HAD2, HAD3, ACY1215, CHR3996, and HAD5 have more hydrogen-bond donors and acceptors, indicating greater potential for polar interactions. ACY1215 and CHR3996 also have the highest acceptor counts, consistent with their strong binding affinity trends. Hydrophobic interaction numbers varied widely, with HAD5 contributing the least. The hydrophobicity ratios indicate that complexes with lower ratios favour polar-driven stabilization. These functional group differences collectively explain the distinct interaction behaviour and binding preferences among the inhibitors.

Table 12. *Amino acid composition of the binding pockets in the HDLP–inhibitor complexes*

	HAD1	**HAD2**	**HAD3**	**HAD4**	**ACY1215**	**CHR3996**	**HAD5**	**SAHA**
Apolar amino acid ratio	0.38	0.42	0.38	0.32	0.32	0.39	0.32	0.39
Polar amino acid ratio	0.40	0.33	0.28	0.36	0.43	0.36	0.45	0.32
Positive amino acid ratio	0.11	0.16	0.17	0.14	0.15	0.13	0.10	0.15
Negative amino acid ratio	0.19	0.17	0.14	0.14	0.18	0.10	0.12	0.12

Table 12 shows distinct variations in amino acid composition among the HDLP binding pockets. ACY1215 and HAD5 display higher polar residue ratios, supporting stronger electrostatic stabilization during binding. Conversely, HAD1 and CHR3996 contain more apolar residues, suggesting greater influence of hydrophobic contacts. Slightly higher proportions of positively charged residues in HAD3 and ACY1215 also favour interaction with negatively charged inhibitor groups. These compositional differences help explain the inhibitor-specific binding preferences and stabilization patterns observed for the HDLP complexes**.**

HDLP–inhibitor interactions with binding pocket residues

DoGSiteScorer was used to identify and characterize potential HDLP binding pockets based on its 3D structure. Pocket size, shape, and

chemical properties are summarized in Tables 8–11, with corresponding druggability scores in Table 12 (0–1 scale, higher values indicate greater suitability for drug-like inhibitors). Residue-specific interactions for HAD1, HAD2, HAD3, HAD4, ACY1215, and SAHA are shown in Figure 8.

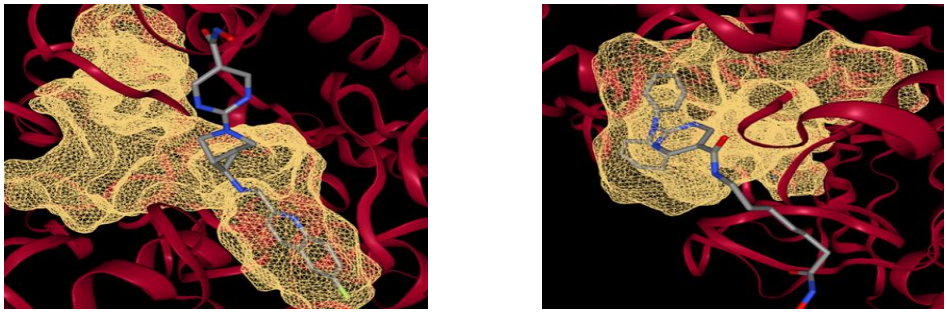

(a) (b)

Figure 8. Interactions between the inhibitor and amino acid residues within the HDLP binding pocket for (a) HDLP–CHR3996 and (b) HDLP–HAD5 complexes.

Table 13. *Drug scores of the binding pockets in the HDLP–inhibitor complexes*

Complex	Pocket	Drug score
HDLP-SAHA	P_0	0.86
	P_1	0.68
HDLP-HAD1	P_0	0.76
	P_2	0.74
HDLP-HAD2	P_0	0.81
	P_1	0.83
HDLP-HAD3	P_0	0.80
	P_2	0.75
HDLP-HAD4	P_0	0.72
	P_3	0.74
HDLP-ACY1215	P_0	0.81

	P_1	0.80
HDLP-CHR3996	P_0	0.84
	P_2	0.72
HDLP-HAD5	P_0	0.80
	P_3	0.77

Table 13 indicates that most HDLP–inhibitor pockets show druggability scores above 0.70, reflecting good compatibility for small-molecule binding. HDLP–SAHA (P_0 = 0.86) and HDLP–CHR3996 (P_0 = 0.84) present the highest drug scores, suggesting that these pockets are highly favourable for ligand accommodation. ACY1215, HAD2, and HAD5 also display strong druggability (>0.80), consistent with their favourable interaction characteristics observed in earlier energy analyses. Overall, these values demonstrate that pocket druggability contributes meaningfully to the binding behaviour of each inhibitor, with CHR3996, SAHA, ACY1215, and HAD2 showing more promising drug-like compatibility within HDLP.

Theoretical estimation of IC_{50} from binding energy

The calculated ΔG_{bind} values obtained from molecular docking were subsequently converted into approximate IC_{50} values using the procedure described in the methodology section. This allowed the inhibitors to be ranked by their predicted inhibitory strength, enabling a clear comparison of potency among the studied compounds.

Table 14. *Estimation of IC_{50} from binding energy obtained from XP docking*

Inhibitor	$\mathbf{\Delta G_{bind}}$ $(\mathbf{kJmol^{-1}})$	$\mathbf{IC_{50} \approx K_i = e^{\frac{\Delta G_{bind}}{RT}}}$	**Potency**
SAHA	-41.53	52 nM	Very good
HAD1	-16.78	1.1 mM	Weak
HAD2	-28.05	12 µM	Low – Moderate
HAD3	-30.78	4 µM	Moderate

HAD4	-21.27	187 μM	Weak
CHR3996	-42.45	36 nM	Very good
ACY1215	-46.41	6.9 nM	Excellent

The binding free energy analysis showed a clear structure–activity relationship among the studied HDAC inhibitors. ACY1215 (ΔG_{bind}= −46.41 kJ mol^{-1}), CHR3996 (−42.45 kJ mol^{-1}), and SAHA (−41.53 kJ mol^{-1}) showed the strongest binding affinities, which correspond to predicted IC_{50} values in the nanomolar range, indicating very high potency and strong suitability as lead candidates. HAD2 and HAD3 exhibited moderate binding affinity, yielding micromolar IC_{50} values, suggesting they may require further structural optimisation to improve inhibitory efficiency. In contrast, HAD1 and HAD4 showed low binding energies, resulting in poor predicted inhibition. Overall, the theoretical ΔG–IC_{50} correlation effectively differentiated between high-, moderate-, and low-potency HDLP inhibitors, supporting the use of computational ΔG estimation as an efficient preliminary screening method before experimental validation.

Conclusions and Recommendations

Comprehensive MD simulations and energetic analyses provided molecular evidence confirming the distinct binding behaviour of HDLP inhibitors. The RMSD, RMSF, SASA, and Rg profiles indicated that CHR3996, ACY1215, and HAD5 formed the most stable complexes, exhibiting reduced structural fluctuations, lower solvent exposure, and consistent compactness throughout the trajectory. CHR3996, in particular, maintained the most stable conformational profile, with minimal deviation and reduced SASA values, indicating tighter binding within the active site. These observations were supported by interaction energy analysis and MM-PBSA results, which showed that CHR3996 had the most favourable non-bonded interaction energy and the most negative binding free energy. Pocket property evaluation also showed that inhibitors binding to moderately sized, deeper pockets had higher affinity, especially for CHR3996 and ACY1215. The functional group and amino acid composition further confirmed that electrostatic complementarity and a balanced distribution of

polar residues significantly contribute to enhanced binding stabilisation.

Additionally, ACY1215, CHR3996, and SAHA displayed the strongest binding free energies and nanomolar IC_{50} values, supporting their potential for further biological prioritization. HAD2 and HAD3 exhibited moderate binding potential with micromolar IC_{50} values, whereas HAD1 and HAD4 were comparatively weak within this inhibitor set. Overall, the ΔG–IC_{50} relationship proved an effective computational screening metric for predicting inhibitor potency before experimental testing.

Based on docking, MD simulations, and MM-PBSA analyses, CHR3996, ACY1215, and possibly HAD5 emerged as the most promising HDAC inhibitors. These computational findings should be validated experimentally through in vitro assays and preclinical studies to confirm efficacy, safety, and pharmacokinetic profiles. Structural optimization may further improve ADMET properties, while future design strategies should focus on minimizing binding site flexibility and maximizing stabilizing interactions. Overall, this study provides a computational framework that can accelerate the discovery and development of HDLP-targeted anticancer therapeutics.

Conflict of Interest

The authors have no conflicts of interest in declaring information that is relevant to the content of this article

References

Agnihotry, S., Pathak, R. K., Singh, D. B., Tiwari, A., & Hussain, I. (2022). Protein structure prediction. *Bioinformatics: Methods and Applications*, 177–188. https://doi.org/10.1016/B978-0-323-89775-4.00023-7

Anbarasu, K., & Jayanthi, S. (2018). Identification of curcumin derivatives as human LMTK3 inhibitors for breast cancer: a docking, dynamics, and MM/PBSA approach. *3 Biotech, 8*(5), 228. https://doi.org/10.1007/s13205-018-1239-6

Chuang, J. C., & Jones, P. A. (2007). Epigenetics and MicroRNAs. *Pediatric Research, 61*(7), 24–29. https://doi.org/10.1203/pdr.0b013e3180457684

Drazic, A., Myklebust, L. M., Ree, R., & Arnesen, T. (2016). The world of protein acetylation. *Biochimica et Biophysica Acta (BBA) - Proteins and Proteomics, 1864*(10), 1372–1401. https://doi.org/10.1016/J.BBAPAP.2016.06.007

Dushanan, R., Weerasinghe, S., Dissanayake, D., & Senthilnithy, R. (2021). An In-Silico Approach to Evaluate the Inhibitory Potency of Selected Hydroxamic Acid Derivatives on Zinc-Dependent Histone Deacetylase Enzyme. *Journal of Computational Biophysics and Chemistry, 20*(6), 603–618. https://doi.org/10.1142/S2737416521500356

Dushanan, R., Weerasinghe, S., Dissanayake, D., & Senthilnithy, R. (2022a). Cracking a Cancer Code Histone Deacetylation in Epigenetic: the Implication from Molecular Dynamics Simulations on Efficacy Assessment of Histone Deacetylase Inhibitors. *Journal of Biomolecular Structure and Dynamics, 40*(5),2352–2368. https://doi.org/10.1080/07391102.2020.1838328

Dushanan, R., Weerasinghe, S., Dissanayake, D., & Senthilnithy, R. (2022b). Driving the New Generation Histone Deacetylase Inhibitors in Cancer Therapy; Manipulation of the Histone Abbreviation at the Epigenetic Level: An In-Silico Approach. *Canadian Journal of Chemistry, 100*(12), 880–890. https://doi.org/10.1139/CJC-2022-0056

Dushanan, R., Weerasinghe, S., Dissanayake, D., & Senthilnithy, R. (2022c). Implication of Ab Initio, QM/MM, and Molecular Dynamics Calculations on the Prediction of the Therapeutic Potential of Some Selected HDAC Inhibitors. *Molecular Simulation,48*(16),1464–1475. https://doi.org/10.1080/08927022.2022.2097672

Dushanan, R., Weerasinghe, S., Dissanayake, D., & Senthilnithy, R. (2025). Cracking a Cancer Code DNA Methylation in Epigenetic Modification: an In-Silico Approach on Efficacy Assessment of Sri Lanka-Oriented Nutraceuticals. *Journal of Biomolecular Structure and Dynamics, 43*(16), 9192–9212. https://doi.org/10.1080/07391102.2024.2321235

Friesner, R. A., Banks, J. L., Murphy, R. B., Halgren, T. A., Klicic, J. J., Mainz, D. T., Repasky, M. P., Knoll, E. H., Shelley, M., Perry, J. K., Shaw, D. E., Francis, P., & Shenkin, P. S. (2004). Glide: A New Approach for Rapid, Accurate Docking and Scoring. 1.

Method and Assessment of Docking Accuracy. *Journal of Medicinal Chemistry, 47*(7), 1739–1749. https://doi.org/10.1021/JM0306430

Frisch, M. J., Trucks, G. W., Schlegel, H. B., Scuseria, G. E., Robb, M. A., Cheeseman, J. R., Scalmani, G., Barone, V., Mennucci, B., Petersson, G. A., Nakatsuji, H., Caricato, M., Li, X., Hratchian, H. P., Izmaylov, A. F., Bloino, J., Zheng, G., Sonnenberg, J. L., Hada, M., … Fox, D. J. (2009). Gaussian 09, Revision A.02 (09). Gaussian, Inc., Wallingford CT. https://www.scirp.org/reference/referencespapers?referenceid=2992136

Nakao, M. (2001). Epigenetics: interaction of DNA methylation and chromatin. *Gene, 278*(1–2), 25–31. https://doi.org/10.1016/S0378-1119(01)00721-1

Nielsen, T. K., Hildmann, C., Dickmanns, A., Schwienhorst, A., & Ficner, R. (2005). Crystal structure of a bacterial class 2 histone deacetylase homologue. *Journal of Molecular Biology, 354*(1), 107–120. https://doi.org/10.1016/j.jmb.2005.09.065

Oostenbrink, C., Soares, T. A., Van Der Vegt, N. F. A., & Van Gunsteren, W. F. (2005). Validation of the 53A6 GROMOS force field. *European Biophysics Journal, 34*(4), 273–284. https://doi.org/10.1007/s00249-004-0448-6

Parthiban, G., Dushanan, R., Weerasinghe, S., Dissanayake, D., & Senthilnithy, R. (2022). Exploration of Novel Mono Hydroxamic Acid Derivatives as Inhibitors for Histone Deacetylase Like Protein (HDLP) by Molecular Dynamics Studies. *Indonesian Journal of Chemistry, 22*(6), 1534–1552. https://doi.org/10.22146/ijc.74167

Paul, A., & Doyle, J. (2004). The old switcheroo: new tricks revealed in 'Phage Lambda Revisited.' *Current Biology, 14*(14), R543–R544. https://doi.org/10.1016/j.cub.2004.07.005

Priyani, P., Samantha, W., Dhammike, D., & Senthilnithy, R. (2021). Impact of Cd(II) on the stability of human uracil DNA glycosylase enzyme; an implication of molecular dynamics trajectories on stability analysis. *Journal of Biomolecular Structure and Dynamics, 40*(24), 1–8. https://doi.org/10.1080/07391102.2021.1999329

Razzak, M. (2013). Allogeneic stem-cell transplantation—resolving questions of timing, remission and the individual. *Nature*

Reviews Clinical Oncology, 10(4), 181–181. https://doi.org/10.1038/nrclinonc.2013.40

Sadri-Vakili, G., & Cha, J.-H. J. (2006). Histone Deacetylase Inhibitors: A Novel Therapeutic Approach to Huntington's Disease (Complex Mechanism of Neuronal Death). *Current Alzheimer Research, 3*(4), 403–408. https://doi.org/10.2174/156720506778249407

Sawatzky, E., Wehle, S., Kling, B., Wendrich, J., Bringmann, G., Sotriffer, C. A., Heilmann, J., & Decker, M. (2016). Discovery of Highly Selective and Nanomolar Carbamate-Based Butyrylcholinesterase Inhibitors by Rational Investigation into Their Inhibition Mode. *Journal of Medicinal Chemistry, 59*(5), 2067–2082. https://doi.org/10.1021/ACS.JMEDCHEM.5B01674/SUPPL_FILE/JM5B01674_SI_002.CSV

Schüttelkopf, A. W., & Van Aalten, D. M. F. (2004). PRODRG: A tool for high-throughput crystallography of protein-ligand complexes. *Acta Crystallographica Section D: Biological Crystallography, 60*(8), 1355–1363. https://doi.org/10.1107/S0907444904011679

Therrien, E., Weill, N., Tomberg, A., Corbeil, C. R., Lee, D., & Moitessier, N. (2014). Docking ligands into flexible and solvated macromolecules. 7. Impact of protein flexibility and water molecules on docking-based virtual screening accuracy. *Journal of Chemical Information and Modeling, 54*(11), 3198–3210. https://doi.org/10.1021/ci500299h

Van Der Spoel, D., Lindahl, E., Hess, B., Groenhof, G., Mark, A. E., & Berendsen, H. J. C. (2005). GROMACS: Fast, flexible, and free. *Journal of Computational Chemistry, 26*(16), 1701–1718. https://doi.org/10.1002/jcc.20291

Wu, X., Zhu, X., Fang, M., Qi, F., Yin, Z., Zhang, J. Z. H., Luo, S., Zhu, T., & Gao, Y. (2025). Insights into Binding Mechanisms of Potential Inhibitors Targeting PCSK9 Protein via Molecular Dynamics Simulation and Free Energy Calculation. *Molecules, 30*(14),2962. https://doi.org/10.3390/MOLECULES30142962/S1